

Micro-Abrasive Wear Behavior Study of an Intermetallic Material—Fe–30Al–6Cr (at.%) Under Conditions of Room and Moderate Temperatures: A Comparison



Eduardo K. T. M. Silva, Jorge H. Luna-Domínguez, Vikas Verma, and Ronaldo Câmara Cozza

Abstract Present work focus on research of tribological resistance of an intermetallic material (Fe–30Al–6Cr—at.%), seeking correlations between wear volume, friction coefficient and temperature. Abrasive experiments were performed with specimens of an iron aluminide alloy against AISI 52100 steel ball and abrasive particles of silicon carbide in glycerin. An individual study was done with respect to their characteristics in terms of SEM-EDS analysis. Different test conditions were defined and the abrasive slurry was, continuously, supplied between the specimen and the ball. Values of tangential force and normal force were acquired simultaneously, for “ball – abrasive particles – specimen” tribological system. Systematic studies of the occurrences of the micro-abrasive wear modes, friction and wear generated during tests were done. Moderate temperature favored a larger degree of plastic deformation than removal of material, reducing the wear rate and decreasing glycerin viscosity, which facilitated the movement of the abrasive particles and, consequently, reduced the friction coefficient. Wear volume presented a rising behavior with increase in sliding distance at room and moderate temperatures. Present research explored the potential of an intermetallic material as structural material subjected to moderate temperatures.

Keywords Iron aluminide alloy · Ball-cratering wear testing · Rolling abrasion

E. K. T. M. Silva · R. C. Cozza (✉)
University Center FEI—Educational Foundation of Ignatius “Priest Sabóia de Medeiros”, São Bernardo do Campo, SP, Brazil
e-mail: rcamara@fei.edu.br

J. H. Luna-Domínguez
Universidad Autónoma de Tamaulipas, Tamaulipas, Mexico

V. Verma
National University of Science and Technology (NUST) MISiS, Moscow, Russia

R. C. Cozza
CEETEPS-State Center of Technological Education “Paula Souza”, Mauá, SP, Brazil

1 Introduction

In recent decades, advantages of use of intermetallic materials in mechanical and metallurgical applications have been observed, mainly aluminide alloys of iron have been researched, primarily due to the possibility of use as structural materials subjected to elevated temperatures [1].

These intermetallic materials exhibit a high concentration of aluminum [1], which form an adherent layer of alumina, protecting materials against corrosion and oxidation under elevated temperatures [1–3]; it also exhibits greater thermodynamic stability than other oxides, as chromium oxide (Cr_2O_3). The intermetallic materials have smaller densities and exhibit excellent mechanical and metallurgical properties [3–5].

The mechanical properties of intermetallic materials can be controlled by varying aluminum percentage, type of heat treatment and the grain size [6, 7], and as a function of these parameters, they can be applied to specific mechanical and metallurgical needs.

Generally, in carbon-steels, decreases in the yield strength stress and the ultimate stress were observed as a function of the increasing temperature; this phenomenon is reported with the maintenance of the value of the Longitudinal Elastic Modulus. However, with the insertion of iron aluminides (Fe_3Al), it is possible to reach a limit of, approximately, 500 °C, while the magnitudes of yield strength stress and ultimate stress either remain constant or increase [8–11].

Regarding wear tests, the tribological test by rotative ball is widely adopted in researches focusing on micro-abrasive wear of various classifications of materials. Figure 1 shows the principle of the tribological test by rotative ball, where a rotative ball is forced against the tested material and an abrasive slurry is fed between the sphere and the specimen during the tests.

“Wear craters” are generated on the tested material and Fig. 2 shows an image of a wear crater, together with a technical indication of the crater diameter (b), which is commonly measured using optical microscopy. The wear volume (V) can

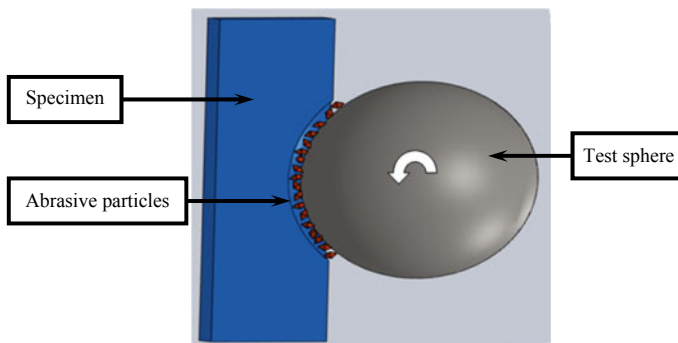
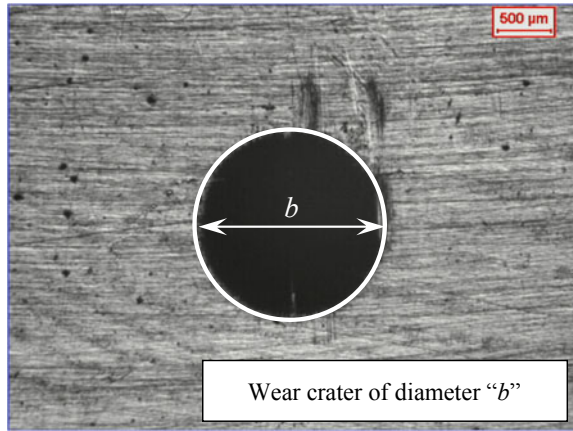


Fig. 1 Ball-cratering tribological test: Its operating principle

Fig. 2 Wear crater from a micro-abrasive wear test by rotative ball: “*b*” is the diameter of the wear crater



be determined as a function of “*b*”, by Eq. (1) [12], being *R* the test sphere radius.

$$V \cong \frac{\pi b^4}{64R} \quad \text{for } b \ll R \tag{1}$$

Generally, two micro-abrasive wear modes are reported on the surface of the wear crater: “*grooving abrasion*” is observed when the abrasive particles slide on the specimen surface (Fig. 3a [13]) and “*rolling abrasion*” is related when the abrasive particles roll along the specimen surface (Fig. 3b).

As published in Reference [14], occurrence of abrasive wear deteriorates the properties and lifespan of engineering components, which are influenced by operational conditions and material properties. Then, the prospective applications of intermetallic materials require characterization and quantification of their tribological properties.

Analyzing the scientific literature regarding to wear of intermetallic materials, is possible to find many works [15–23]. However, researches on the micro-abrasive

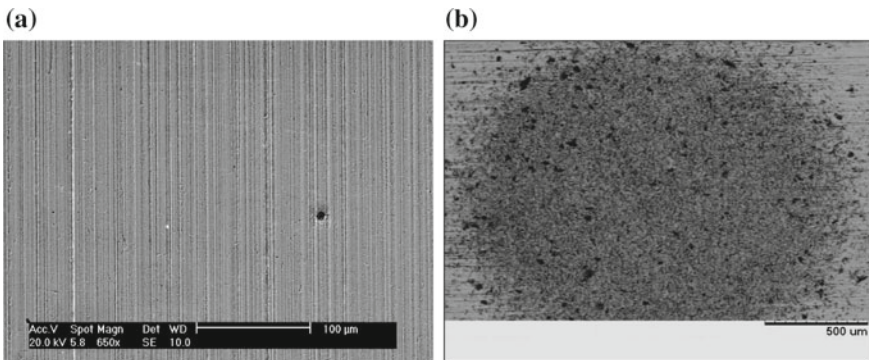


Fig. 3 Micro-abrasive wear modes: a “*grooving abrasion*” [13] and b “*rolling abrasion*”

wear behavior of intermetallic materials under room and moderate temperatures are scarce. Then, considering the importance of intermetallic materials in many industrial applications [24–31], the purpose of this work is to characterize the micro-abrasive wear performance of an intermetallic material under room and moderate temperatures, seeking correlations between wear volume, friction coefficient and temperature.

2 Materials and Methods

2.1 Tribometer

Analyzing possible (micro-)abrasive wear test methods to conduct this research, “ball-cratering” procedure provided a favorable technical condition to conduct micro-abrasive wear study under room and moderate temperatures, due to its mechanical set.

Thus, a ball-cratering wear test equipment of “free-ball” mechanical configuration (Fig. 4) was used to conduct tribological tests at room and moderate temperatures. To heat the intermetallic material and conduct experiments above room temperature, a device consisting of an aluminum specimen-support block containing a 1.2 kW electrical heating element was coupled to equipment. Additionally, two load cells were used: one lead cell to control the “normal force— N ” and one load cell to measure the “tangential force— T ”.

Fig. 4 Ball-cratering equipment of “free-ball” configuration

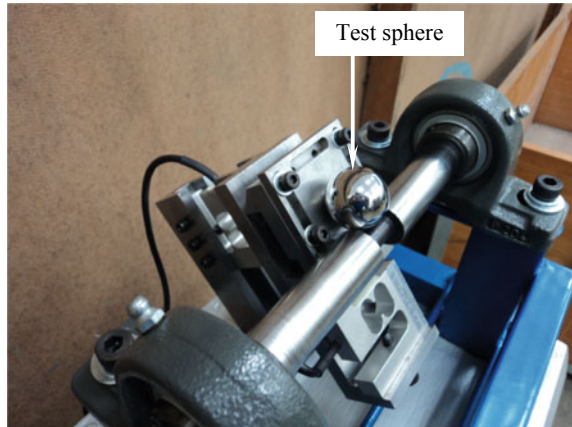
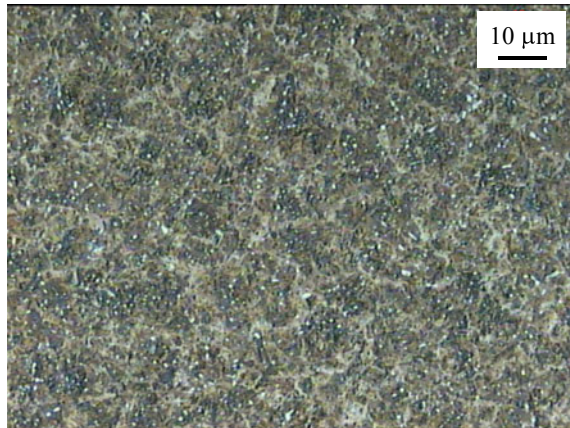


Fig. 5 AISI 52100 bearing steel sphere quenched in oil at 860 °C and stress-relieved at 200 °C for 1 h: its microstructure and chemical composition [32–34]



Chemical Element	% (in weight)
C	1.04
Mn	0.35
Si	0.25
Cr	1.45
Fe	Balance

2.2 Tested Intermetallic Material

The tested material was an intermetallic material—Fe–30Al–6Cr (at.%), researched in the “*as cast*” state.

The tested iron aluminide alloy was characterized by SEM and EDS.

2.3 Counter-Body

An AISI 52100 bearing steel ball was used as counter-body; its diameter was $D = 1''$ ($D = 25.4$ mm—*standard size*).

Figure 5 [32–34] shows an image of its microstructure with the respective chemical composition.

2.4 Abrasive Slurries

The abrasive slurry was composed by abrasive particles of silicon carbide and glycerin.

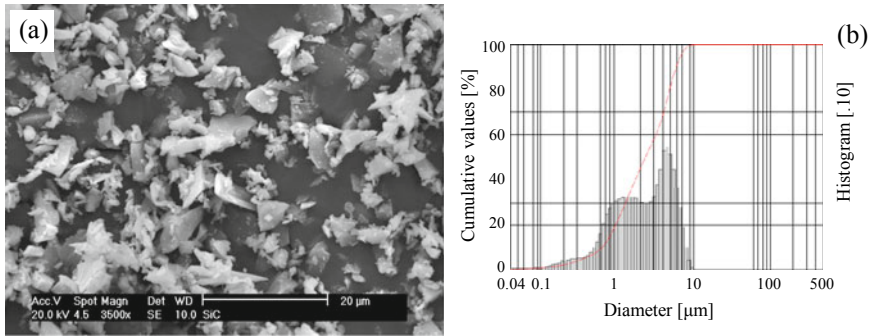


Fig. 6 Abrasive particles of SiC [33, 34]: **a** image obtained by scanning electron microscopy (SEM) and **b** its particle size distribution

Table 1 Hardness of the materials used in this research [7, 8, 32–34]

	Material	Hardness— H [HV]	
Tested material	Fe–30Al–6Cr (at.%) intermetallic material	381.6	[7, 8]
Test sphere	AISI 52100 bearing steel	856	[32–34]
Abrasive material	Black silicon carbide—SiC	1886–1937	[33, 34]

SiC material presented an average particle size of 3 μm and an angular shape. Figure 6 [33, 34] shows a scanning electron micrograph of the abrasive material (Fig. 6a) and its particle size distribution (Fig. 6b).

2.5 Hardness of the Materials

Table 1 presents the hardness (H) of the materials used in this research (intermetallic material [7, 8], test ball [32–34] and abrasive particles [33, 34]).

2.6 Experiments

Table 2 presents the tribological parameters defined for the performed tribological tests.

One value for normal force (N) was selected, $N = 0.40$ N, together with one value of abrasive slurry concentration (C), $C = 35\%$ SiC + 65% glycerin (volumetric values) and two values for the test temperatures (T_e), $T_{e1} = 29$ °C (room temperature) and $T_{e2} = 250$ °C (moderate temperature).

Table 2 Test parameters established for the tribological tests

Normal force	[N]	N	0.4
Abrasive slurry concentration	(% vol)	C	35% SiC + 65% glycerin
Temperature of test	[°C]	Te_1	29 (room)
		Te_2	250 (moderate)
Test sphere rotational speed	[rpm]	n	75
Tangential sliding velocity of the test sphere	[m/s]	v	0.1
Sliding distance	[m]	S_1	6
		S_2	12
		S_3	24
Test time	[min]	t_1	1
		t_2	2
		t_3	4

The test ball rotational speed was $n = 75$ rpm, previously selected by other Researchers [35–37]. For $n = 75$ rpm and a ball of diameter $D = 1$ ”, its tangential sliding velocity is $v = 0.1$ m/s.

Three values of sliding distance (S) were established: $S_1 = 6$ m, $S_2 = 12$ m and $S_3 = 24$ m, with the following corresponding test times (t): $t_1 = 1$ min, $t_2 = 2$ min and $t_3 = 4$ min. Three tribological tests were conducted for each value of sliding distance, according to the following test sequence: 6–6–24–12–12–24–24–12 and 6 m. In total, 18 tribological tests were conducted: nine experiments at $Te_1 = 29$ °C (room temperature) and nine experiments at $Te_2 = 250$ °C (moderate temperature).

All tribological experiments were conducted without interruption. Additionally, the test temperature of $Te_2 = 250$ °C was monitored using an infrared thermometer.

2.7 Results Analysis

With the aim of measuring the dimension “ b ” of each wear crater and reporting the occurrences of the abrasive wear modes, subsequently at the end of wear tests, the wear craters were analyzed by optical microscopy and scanning electron microscopy, respectively.

Then, with the values of “ b ”, “ T ” and “ N ”, volume of wear (V) and friction coefficient (μ) were determined using Eqs. (1) and (2), respectively.

$$\mu = \frac{T}{N} \tag{2}$$

Finally, graphs of $V = f(S, Te)$ and $\mu = f(t, Te)$ were plotted to shows the results obtained.

3 Results and Discussion

3.1 Intermetallic Material Characterization

Figures 7a [7, 8] and 7b [8] are the micrographs (SEM) of the iron aluminide alloy studied; its surface was etched using Vilella’s reagent (composition of 95 ml of ethanol, 5 ml of HCl and 1 g of picric acid). It consists of an aluminide matrix (D03 ordered) reinforced by a continuous network of eutectic chromium carbides at the interdendritic regions, tentatively identified as M_7C_3 based on the chromium/iron ratio measured by EDS, where Figs. 7c [8] and 7d [8] show the results obtained, for the “as cast” state and region of carbides.

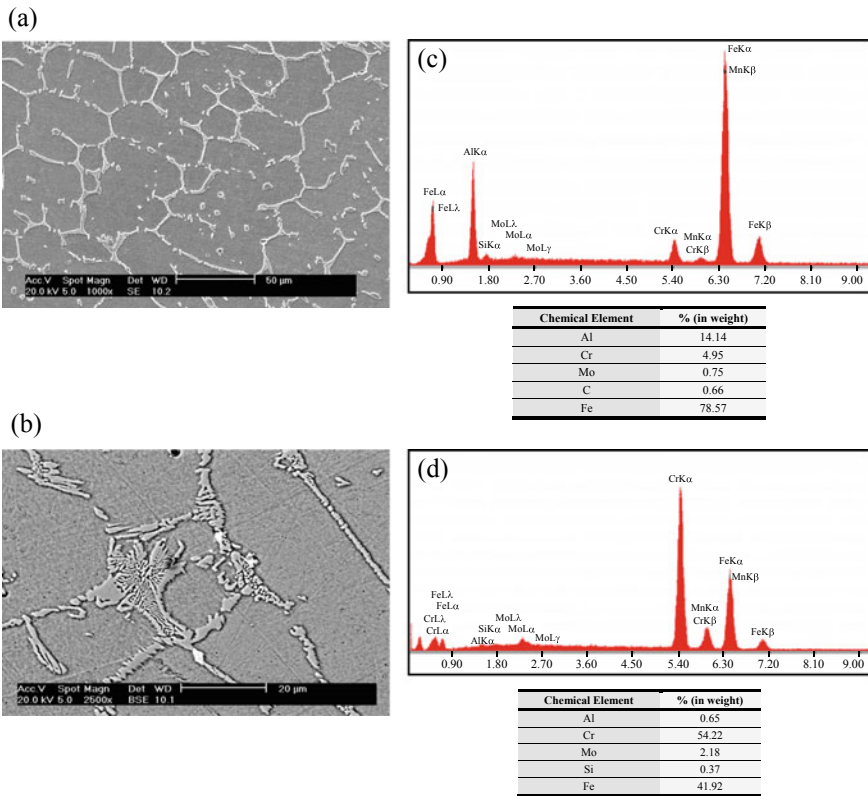


Fig. 7 Fe-30Al-6Cr (at.%) intermetallic material: **a–b** Its microstructure [7, 8] and EDS for the **c** “as cast” state [8] and **d** region of carbides [8]

3.2 Micro-Abrasive Wear Modes Analysis

Figure 8a shows a wear crater produced during the ball-cratering tribological experiments by rotative ball. Figure 8b, c show images obtained by SEM, where the occurrence of rolling abrasion is observed for the conditions of $Te_1 = 29\text{ }^\circ\text{C}$ and $Te_2 = 250\text{ }^\circ\text{C}$, respectively.

Independent of the sliding distance and test temperature, in all experimental conditions, the wear craters exhibited the occurrence of rolling abrasion. This tribological behavior is in qualitative agreement with the results reported in the literature [35–40], including reports that low values of normal forces and high values of abrasive slurries concentrations favor the occurrence of rolling abrasion.

The greater propensity of rolling abrasion action in the tests conducted under elevated temperature can be explained by the fact that upon increasing the temperature, the specimen material became more ductile, facilitating its indentation by the SiC abrasive particles.

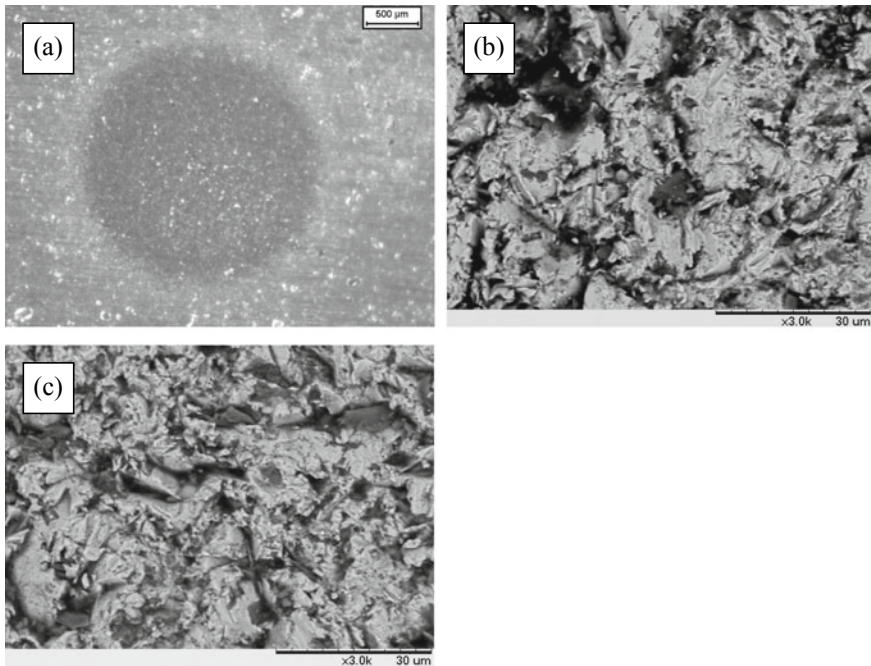


Fig. 8 a Wear crater produced during the ball-cratering tribological experiments ($Te_1 = 29\text{ }^\circ\text{C}$) and the action of rolling abrasion for the conditions of b $Te_1 = 29\text{ }^\circ\text{C}$ and c $Te_2 = 250\text{ }^\circ\text{C}$

3.3 Micro-Abrasive Wear Modes Analysis

The behaviors of the wear volume (V) as a function of the sliding distance (S) and temperature (Te) – $V = f(S, Te)$ are presented in Fig. 9.

In both cases, the wear volume presented a rising behavior with the increase of the sliding distance. In addition, the reproducibility obtained in the experiments of this work was directly influenced by the action of rolling abrasion in the wear craters, which, as reported by Bose and Wood [41], tends to produce results with relatively reliable reproducibility.

By analyzing Fig. 9, it is possible to note that the wear volume decreased with the increase of the test temperature— Te .

The rolling abrasion, which is the abrasive wear observed in all wear craters of this work, can be related to the “cutting” and “micro-fatigue” [42] that occurs due to repetitive rolling of the abrasive particles on the surface of the wear crater, e.g., the wear that occurs due to plastic deformation [43].

With the increase in the temperature, the material of the specimen exhibits larger ductility, consequently favoring a larger degree of plastic deformation than removal of material. This high capacity of plastic deformation that the specimen material acquires with the increase of the test temperature favors the occurrence of “micro-fatigue” (due to the actions of the abrasive particles) which, in addition to being the wear mechanism of smaller severity when compared with the “cutting”, is consequently associated with smaller wear rates. To remove a certain quantity of material under the occurrence of micro-fatigue (plastic deformation), a larger number of abrasive particles must slide or to roll in the same region of wear.

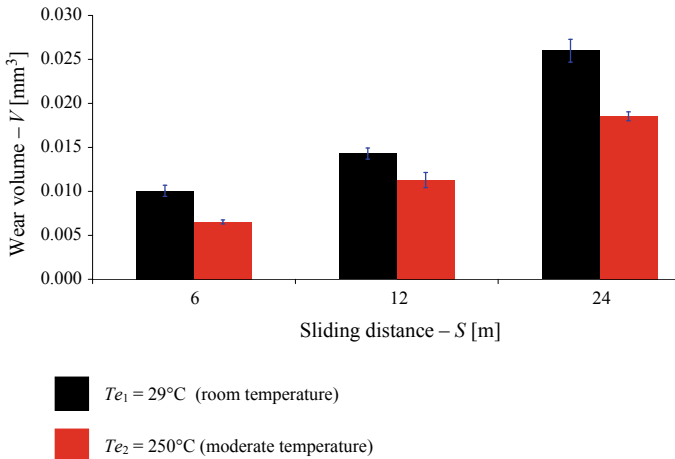


Fig. 9 Wear volume (V) as a function of the sliding distance (S) and the temperature of test (Te) – $V = f(S, Te)$

3.4 Friction Coefficient Analysis

Figure 10 shows the graphics of the friction coefficient (μ) as a function of the test time (t) and test temperature (Te) – $\mu = f(t, Te)$.

Independent of the test condition, the friction coefficient tended to a constant behavior as a function of the test time and temperature.

The temperature significantly influenced the values of the friction coefficient, and in a general overview, the coefficient of friction obtained under $Te_1 = 29^\circ\text{C}$ was found to be greater than the values of μ obtained under $Te_2 = 250^\circ\text{C}$. With the increase in the temperature, the specimen material becomes more ductile; thus, a greater amount of abrasive particles is required to rub on a wear region to remove the same quantity of material. In addition, an abrasive particle is more likely to cut at room temperature, while an abrasive particle just deforms plastically under an elevated temperature. Finally, with the increase in the temperature, the viscosity of the glycerin decreased, facilitating the movement of the abrasive particles and, consequently, decreasing the friction coefficient.

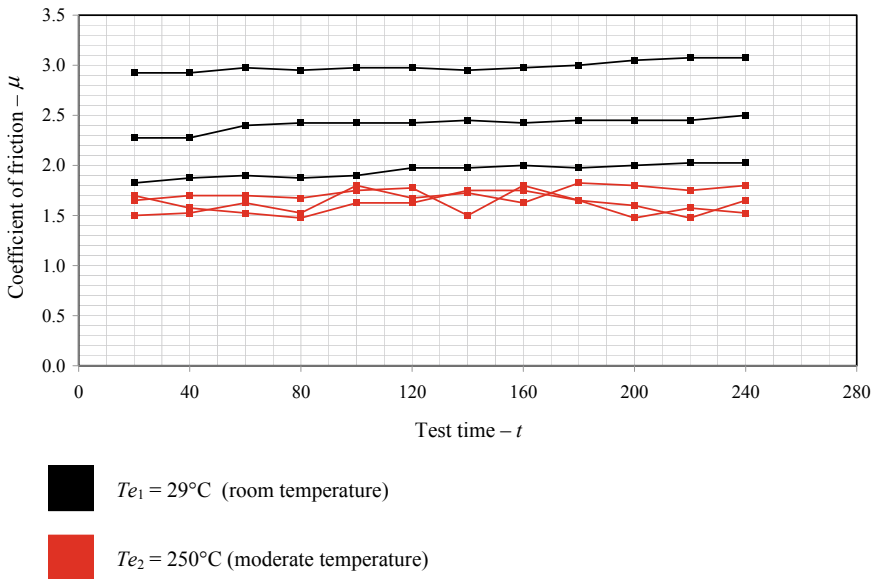


Fig. 10 Graphics of the friction coefficient (μ) as a function of the test time (t) and test temperature (Te) – $\mu = f(t, Te)$

4 Conclusions

Present research explored the potential of an iron aluminide alloy as structural materials subjected to moderate temperatures.

The following points can be highlighted in this research:

- The action of the “*rolling abrasion*” micro-abrasive wear mode was independent of the temperature of test;
- The temperature significantly influences the tribological behavior of the Fe-30Al-6Cr (at.%) intermetallic material studied: as the temperature increased, the wear resistance of the alloy increased;
- Wear volume and friction coefficient: as the temperature increased, the wear volume and the friction coefficient decreased due to the higher ductility acquired by the material specimen and lower viscosity of the glycerin.

References

1. Morris DG, Morris-Muñoz MA (1999) The influence of microstructure on the ductility of iron aluminides. *Intermetallics* 7(10):1121–1129. [https://doi.org/10.1016/S0966-9795\(99\)00038-2](https://doi.org/10.1016/S0966-9795(99)00038-2)
2. Risanti DD, Sauthoff G (2011) Microstructures and mechanical properties of Fe-Al-Ta alloys with strengthening Laves phase. *Intermetallics* 19(11):1727–1736. <https://doi.org/10.1016/j.intermet.2011.07.008>
3. Hanus P, Bartsch E, Palm M, Krein R, Bauer-Partenheimer K, Janschek P (2010) Mechanical properties of a forged Fe-25Al-2Ta steam turbine blade. *Intermetallics* 18(7):1379–1384. <https://doi.org/10.1016/j.intermet.2009.12.035>
4. Wu D, Baker I, Munroe PR, George EP (2007) The yield strength anomaly of single-slip-oriented Fe-Al single crystals. *Intermetallics* 15(2):103–107. <https://doi.org/10.1016/j.intermet.2006.03.007>
5. Krein R, Schneider A, Sauthoff G, Frommeyer G (2007) Microstructure and mechanical properties of Fe₃Al-based alloys with strengthening boride precipitates. *Intermetallics* 15(9):1172–1182. <https://doi.org/10.1016/j.intermet.2007.02.005>
6. Herrmann J, Inden G, Sauthoff G (2003) Deformation behavior of iron-rich iron-aluminium alloys at high temperatures. *Acta Mater* 51(11):3233–3242. [https://doi.org/10.1016/S1359-6454\(03\)00144-7](https://doi.org/10.1016/S1359-6454(03)00144-7)
7. Borges DFL, Espinosa DCR, Schön CG (2014) Making iron aluminides out of scrap. *J Mater Res Technol* 3(2):101–106. <https://doi.org/10.1016/j.jmrt.2013.12.002>
8. Borges DFL (2010) Processing and characterization of iron aluminides made from recycled raw materials (master’s thesis, Polytechnic School of the University of São Paulo, São Paulo—SP, Brazil, 2010). Available online: <http://www.teses.usp.br/teses/disponiveis/3/3133/tde-25102011-122243/pt-br.php>
9. Guan X, Iwasaki K, Kishi K, Yamamoto M, Tanaka R (2004) Dry sliding wear behavior of Fe-28Al and Fe-28Al-10Ti alloys. *Mater Sci Eng A* 366(1):127–134. <https://doi.org/10.1016/j.msea.2003.09.049>
10. Zhang X, Ma J, Fu L, Zhu S, Li F, Yang J, Liu W (2013) High temperature wear resistance of Fe-28Al-5Cr alloy and its composites reinforced by TiC. *Tribol Int* 61:48–55. <https://doi.org/10.1016/j.triboint.2012.12.005>

11. Sharma G, Limaye PK, Ramanujan RV, Sundararaman M, Prabhu N (2004) Dry-sliding wear studies of Fe₃Al-ordered intermetallic alloy. *Mater Sci Eng, A* 386(1–2):408–414. <https://doi.org/10.1016/j.msea.2004.07.053>
12. Rutherford KL, Hutchings IM (1997) Theory and application of a micro-scale abrasive wear test. *J Test Eval JTEVA* 25(2):250–260. [doi.org/doi.org/10.1520/JTE11487J](https://doi.org/10.1520/JTE11487J)
13. Cozza RC, Tanaka DK, Souza RM (2009) Friction coefficient and abrasive wear modes in ball-cratering tests conducted at constant normal force and constant pressure—preliminary results. *Wear* 267(1–4):61–70. <https://doi.org/10.1016/j.wear.2009.01.055>
14. Sapate SG, Selokar A, Garg N (2010) Experimental investigation of hardfaced martensitic steel under slurry abrasion conditions. *Mater Des* 31(8):4001–4006. <https://doi.org/10.1016/j.matdes.2010.03.009>
15. Itoi T, Mineta S, Kimura H, Yoshimi K, Hirohashi M (2010) Fabrication and wear properties of Fe₃Al-based composites. *Intermetallics* 18(11):2169–2177. <https://doi.org/10.1016/j.intermet.2010.07.014>
16. Józwiak S, Karczewski K (2009) Influence of aluminum oxides on abrasive wear resistance of Fe-50 at.% Al intermetallics sinters. *J Alloy Compd* 482(1–2):405–411. <https://doi.org/10.1016/j.jallcom.2009.04.034>
17. Malafaia AMS, Milan MT, Omar M, Muñoz Rıofano RM, de Oliveira MF (2010) Oxidation and abrasive wear of Fe-Si and Fe-Al intermetallic alloys. *J Mater Sci* 45(19):5393–5397. <https://doi.org/10.1007/s10853-010-4591-4>
18. Johnson M, Mikkola DE, March PA, Wright RN (1990) The resistance of nickel and iron aluminides to cavitation erosion and abrasive wear. *Wear* 140(2):279–289. [https://doi.org/10.1016/0043-1648\(90\)90090-W](https://doi.org/10.1016/0043-1648(90)90090-W)
19. Ahmadian M, Wexler D, Chandra T, Calka A (2005) Abrasive wear of WC-FeAl-B and WC-Ni₃Al-B composites. *Int J Refract Metal Hard Mater* 23(3):155–159. <https://doi.org/10.1016/j.ijrmhm.2004.12.002>
20. Mosbah AY, Wexler D, Calka A (2005) Abrasive wear of WC-FeAl composites. *Wear* 258(9):1337–1341. <https://doi.org/10.1016/j.wear.2004.09.061>
21. Alman DE, Hawk JA, Tylczak JH, Doğan CP, Wilson RD (2001) Wear of iron-aluminide intermetallic-based alloys and composites by hard particles. *Wear* 251(1–12):875–884. [https://doi.org/10.1016/S0043-1648\(01\)00745-1](https://doi.org/10.1016/S0043-1648(01)00745-1)
22. Hawk JA, Alman DE (1997) Abrasive wear of intermetallic-based alloys and composites. *Mater Sci Eng, A* 239–240:899–906. [https://doi.org/10.1016/S0921-5093\(97\)00681-3](https://doi.org/10.1016/S0921-5093(97)00681-3)
23. Maupin HE, Wilson RD, Hawk JA (1992) An abrasive wear study of ordered Fe₃Al. *Wear* 159(2):241–247. [https://doi.org/10.1016/0043-1648\(92\)90307-T](https://doi.org/10.1016/0043-1648(92)90307-T)
24. Aoki K (1990) Ductilization of L1₂ intermetallic compound Ni₃Al by microalloying with boron: materials transactions. *JIM* 31(6):443–448. <https://doi.org/10.2320/matertrans1989.31.443>
25. Deevi SC, Sikka VK (1996) Nickel and iron aluminides: an overview on properties, processing, and applications. *Intermetallics* 4(5):357–375. [https://doi.org/10.1016/0966-9795\(95\)00056-9](https://doi.org/10.1016/0966-9795(95)00056-9)
26. Morris DG (1998) Possibilities for high-temperature strengthening in iron aluminides. *Intermetallics* 6(7–8):753–758. [https://doi.org/10.1016/S0966-9795\(98\)00028-4](https://doi.org/10.1016/S0966-9795(98)00028-4)
27. Schneibel JH, George EP, Anderson IM (1997) Tensile ductility, slow crack growth, and fracture mode of ternary B2 iron aluminides at room temperature. *Intermetallics* 5(3):185–193. [https://doi.org/10.1016/S0966-9795\(96\)00087-8](https://doi.org/10.1016/S0966-9795(96)00087-8)
28. Dobeš F, Milička K (2010) Estimation of ductility of Fe-Al alloys by means of small punch test. *Intermetallics* 18(7):1357–1359. <https://doi.org/10.1016/j.intermet.2009.11.002>
29. Stein F, Schneider A, Frommeyer G (2003) Flow stress anomaly and order-disorder transitions in Fe₃Al-based Fe-Al-Ti-X alloys with X = V, Cr, Nb, or Mo. *Intermetallics* 11(1):71–82. [https://doi.org/10.1016/S0966-9795\(02\)00187-5](https://doi.org/10.1016/S0966-9795(02)00187-5)
30. Morris DG, Chao J, Garcia Oca C, Muñoz-Morris MA (2003) Obtaining good ductility in an FeAl intermetallic. *Mater Sci Eng A* 339(1–2):232–240. [https://doi.org/10.1016/S0921-5093\(02\)00108-9](https://doi.org/10.1016/S0921-5093(02)00108-9)

31. Bystrzycki J, Fraczkiewicz A, Łyszkowski R, Mondon M, Pakiela Z (2010) Microstructure and tensile behavior of Fe-16Al-based alloy after severe plastic deformation. *Intermetallics* 18(7):1338–1343. <https://doi.org/10.1016/j.intermet.2010.01.014>
32. Cozza RC (2013) A study on friction coefficient and wear coefficient of coated systems submitted to micro-scale abrasion tests. *Surf Coat Technol* 215:224–233. <https://doi.org/10.1016/j.surfcoat.2012.06.088>
33. Cozza RC, Tanaka DK, Souza RM (2011) Friction coefficient and wear mode transition in micro-scale abrasion tests. *Tribol Int* 44(12):1878–1889. <https://doi.org/10.1016/j.triboint.2011.08.006>
34. Cozza RC (2014) Influence of the normal force, abrasive slurry concentration and abrasive wear modes on the coefficient of friction in ball-cratering wear tests. *Tribol Int* 70:52–62. <https://doi.org/10.1016/j.triboint.2013.09.010>
35. Adachi K, Hutchings IM (2003) Wear-mode mapping for the micro-scale abrasion test. *Wear* 255(1–6):23–29. [https://doi.org/10.1016/S0043-1648\(03\)00073-5](https://doi.org/10.1016/S0043-1648(03)00073-5)
36. Adachi K, Hutchings IM (2005) Sensitivity of wear rates in the micro-scale abrasion test to test conditions and material hardness. *Wear* 258(1–4):318–321. <https://doi.org/10.1016/j.wear.2004.02.016>
37. Trezona RI, Allsopp DN, Hutchings IM (1999) Transitions between two-body and three-body abrasive wear: influence of test conditions in the microscale abrasive wear test. *Wear* 225–229:205–214. [https://doi.org/10.1016/S0043-1648\(98\)00358-5](https://doi.org/10.1016/S0043-1648(98)00358-5)
38. Mergler YJ, in't Veld AH (2003) Micro-abrasive wear of semi-crystalline polymers. *Tribol Res Des Eng Syst* 41:165–173. [https://doi.org/10.1016/S0167-8922\(03\)80129-3](https://doi.org/10.1016/S0167-8922(03)80129-3)
39. Umemura MT, Varela LB, Pinedo CE, Cozza RC, Tschiptschin AP (2019) Assessment of tribological properties of plasma nitrided 410S ferritic-martensitic stainless steels. *Wear* 426–427:49–58. <https://doi.org/10.1016/j.wear.2018.12.092>
40. Allsopp DN, Hutchings IM (2001) Micro-scale abrasion and scratch response of PVD coatings at elevated temperatures. *Wear* 251(1–12):1308–1314. [https://doi.org/10.1016/S0043-1648\(01\)00755-4](https://doi.org/10.1016/S0043-1648(01)00755-4)
41. Bose K, Wood RJK (2005) Optimum tests conditions for attaining uniform rolling abrasion in ball cratering tests on hard coatings. *Wear* 258(1–4):322–332. <https://doi.org/10.1016/j.wear.2004.09.018>
42. Axén N, Jacobson S, Hogmark S (1994) Influence of hardness of the counterbody in three-body abrasive wear—an overlooked hardness effect. *Tribol Int* 27(4):233–241. [https://doi.org/10.1016/0301-679X\(94\)90003-5](https://doi.org/10.1016/0301-679X(94)90003-5)
43. Fang L, Liu W, Du D, Zhang X, Xue Q (2004) Predicting three-body abrasive wear using Monte Carlo methods. *Wear* 256(7–8):685–694. [https://doi.org/10.1016/S0043-1648\(03\)00464-2](https://doi.org/10.1016/S0043-1648(03)00464-2)